

Melting of a 2D Quantum Electron Solid in High Magnetic Field

Yong P. Chen,^{1,2,*} G. Sambandamurthy,^{2,1} Z. H. Wang,^{3,2} R. M. Lewis,^{2,1,†}
L. W. Engel,² D. C. Tsui,¹ P. D. Ye,^{2,1,‡} L. N. Pfeiffer,⁴ and K. W. West⁴

¹*Department of Electrical Engineering, Princeton University, Princeton, NJ 08544*

²*National High Magnetic Field Laboratory, 1800 E. Paul Dirac Drive, Tallahassee, FL 32310*

³*Department of Physics, Princeton University, Princeton, NJ 08544*

⁴*Bell Laboratories, Lucent Technology, Murray Hill, NJ 07974*

The melting temperature (T_m) of a solid is generally determined by the pressure applied to it, or indirectly by its density (n) through the equation of state. This remains true even for helium solids¹, where quantum effects often lead to unusual properties². In this letter we present experimental evidence to show that for a two dimensional (2D) solid formed by electrons in a semiconductor sample under a strong perpendicular magnetic field³ (B), the T_m is not controlled by n , but effectively by the *quantum correlation* between the electrons through the Landau level filling factor $\nu = nh/eB$. Such melting behavior, different from that of all other known solids (including a classical 2D electron solid at zero magnetic field⁴), attests to the quantum nature of the magnetic field induced electron solid. Moreover, we found the T_m to increase with the strength of the sample-dependent disorder that pins the electron solid.

Electrons are expected to crystalize into a solid (so called “Wigner crystal”⁵) when the (Coulomb) interaction energy between the electrons sufficiently dominates over the kinetic energy. One example of such an electron solid was found in a very low density (n) two dimensional electron system (2DES) realized on helium surfaces⁴ (at zero magnetic field). Because of the low n , the zero-point motion (given by the Fermi energy $E_f = nh^2/2\pi m$ where m is the electron mass) is negligibly small and at finite temperatures (T), as in the experiment⁴, the kinetic energy originates mainly from the *classical* thermal motion ($k_B T$). The melting of such a “classical” 2D electron solid is determined only by the competition between the thermal kinetic energy and Coulomb interaction ($e^2\sqrt{n}/4\pi\epsilon$) [MKS unit is used exclusively in this paper] and is thought to be describable by the Kosterlitz-Thouless theory of 2D melting⁶. Experimentally, the melting was found to occur⁴ at $T_{cm} = e^2\sqrt{n}/(4\pi\epsilon k_B\Gamma)$ (where ϵ is the dielectric constant and k_B the Boltzmann constant) with $\Gamma \sim 130$, in excellent agreement with theoretical calculations^{7,8}.

The 2DES as realized in high-quality GaAs/AlGaAs structures in our experiment has relatively high n , thus (in the absence of magnetic fields) the zero-point motion (E_f) is significant and the 2DES does not solidify even at $T=0$. However, it is well known that a sufficiently strong perpendicular magnetic field (B) tends to suppress the kinetic energy of 2D electrons and in-

duce the solidification^{9,10}. On the other hand, at finite B the motion of electrons is quantized into Landau levels (LL) and delicate many-body quantum correlations^{11,12} among electrons can cause the 2DES to condense into fractional quantum Hall (FQH)¹³ liquid states at certain rational fractional values of Landau level filling factor $\nu = nh/eB$. Experimentally, the “magnetic field induced electron solid” (MIES)³ forms at sufficiently small ν , following the termination of FQH states at low T . It is deformed and pinned by disorder in the system, thus an insulator (in DC transport), and has a characteristic resonance (see, for example, Ref. 14) in its frequency (f) dependent, real diagonal conductivity ($\text{Re}[\sigma_{xx}(f)]$) due to the “pinning mode” of domains of the elastic solid oscillating collectively around the disorder^{15,16,17}.

The melting of such a MIES has been studied in various experiments^{18,19,20,21,22,23} and it was commonly presumed^{8,18,20,22} that at a fixed ν the melting should be similar to that of a classical electron solid (the expected exact ground state for a 2DES at infinite B) and thus T_m would be determined by n , as T_{cm} is. In this letter, we show unambiguously that this is not the case, that is, the melting of a MIES does *not* behave as a classical electron solid, and in fact in any given sample (whose intrinsic disorder is fixed), T_m is determined by ν , not n , and is unrelated to T_{cm} .

In our experiments we have studied the T -dependence of the pinning mode resonance of the MIES in its $\text{Re}[\sigma_{xx}(f)]$ spectrum measured by microwave spectroscopy²⁴. No resonance is observed when T is raised above some characteristic T_m , taken as the melting T of the electron solid. By systematically measuring T_m while varying *both* n and B , we found that within the experimental resolution, T_m in a given sample is only a function of ν (i.e., $T_m(n, B) = T_m(n/B)$) down to ν as small as ~ 0.05 attained in our experiments. Although T_m is generally sensitive to n at fixed B , T_m is *insensitive* to n at fixed ν . Since $\nu = nh/eB = 2(l_B/r)^2$, where the magnetic length $l_B = \sqrt{\hbar/eB}$ is a measure of the size of the single electron wavefunction and $r = 1/\sqrt{\pi n}$ is the mean separation between the electrons, our findings reflect the quantum nature of the 2D electron solid formed at finite B and demonstrate that its melting (T_m) is effectively controlled by the inter-electron quantum correlation, which depends on l_B/r .

We have studied two different 2DES samples. Sample 1 is a GaAs/AlGaAs heterojunction. Sample 2 is a 15nm-wide AlGaAs/GaAs/AlGaAs quantum well (QW).

By backgating and/or different cooldowns, the electron densities (n) in both samples can be tuned to various extents (to be specified below). Typically at their respective as-cooled n , sample 1 has mobility $\mu \sim 6 \times 10^6$ cm²/Vs, sample 2 has $\mu \sim 1 \times 10^6$ cm²/Vs.

The inset of Fig. 1(b) shows a schematic local cross section of a typical sample (not to scale). A metal film coplanar waveguide (CPW), lithographically deposited on the surface, enables the measurement of $\text{Re}[\sigma_{xx}(f)]$ of the 2DES. A network analyzer generates a microwave signal propagating along the CPW and coupling capacitively to the 2DES (located some 0.1-0.5 μm below the surface). The relative power absorption (P) by the 2DES is measured and can be related²⁴ to $\text{Re}[\sigma_{xx}]$ of the 2DES as $P = \exp((2lZ_0/w)\text{Re}[\sigma_{xx}])$, where l and w are the total length and slot width of the CPW respectively and $Z_0 = 50\Omega$ is the CPW characteristic impedance. CPW of meander shapes²⁴ are commonly used to obtain larger geometric ratios ($2l/w$), and therefore to increase the strength of the signal (P). The sample is mounted on a metal block that is kept in good thermal equilibrium with the mixing chamber of a dilution refrigerator during the measurements. The microwave input is kept in the low power limit, by reducing the power till the signal (P) no longer changes. A negative voltage between a backgate (located ~ 200 μm below the surface) and the 2DES enables *in-situ* reduction of n from the as-cooled values.

Fig. 1 shows T -dependence of the microwave resonance of the electron solid in sample 1 and the determination of T_m at two different values of n with ν fixed at a representative value of 0.128. In Fig. 1a, $n = 5.6 \times 10^{10}$ cm⁻² ($B = 18$ T) and the $\text{Re}[\sigma_{xx}(f)]$ spectrum displays a clear resonance with peak frequency (f_{pk}) near 600 MHz at low T (~ 50 mK). As T is increased, the resonance weakens. Its f_{pk} at elevated T also decreases slightly from the base T (50 mK) value, but by no more than 20%, indicating that there is no significant loss of pinning of the electron solid due to the increase of the temperature. The resonance disappears into noise background at ~ 250 mK, which we take as the melting T (T_m) of the electron solid. The inset of Fig. 1a shows that the resonance amplitude (obtained from a Lorentzian fit) extrapolates to zero at a similar T_m . In Fig. 1b, n has been reduced to 2.1×10^{10} cm⁻² (using a backgate voltage of -300 V) while B is also reduced to 6.86 T to keep ν the same value as in Fig. 1a. The lower n reduces the electron-electron interaction relative to the electron-disorder interaction, and the pinning resonance of the electron solid now occurs (at low T) near 1.6 GHz, which is significantly higher than that in Fig. 1a. However, the resonance disappears above a $T_m \sim 270$ mK, which is similar to the T_m in Fig. 1a, within the experimental uncertainty in determining T_m (typically $\sim 10\%$).

We have measured T_m in 4 different cooldowns of sample 1 for many combinations of n and B , at which a resonance from the MIES can be detected. We plot all these T_m data as a function of ν in Fig. 2. Sample 1 has a particularly large range of tunable n , from $\sim 1.2 - 8.1 \times 10^{10}$

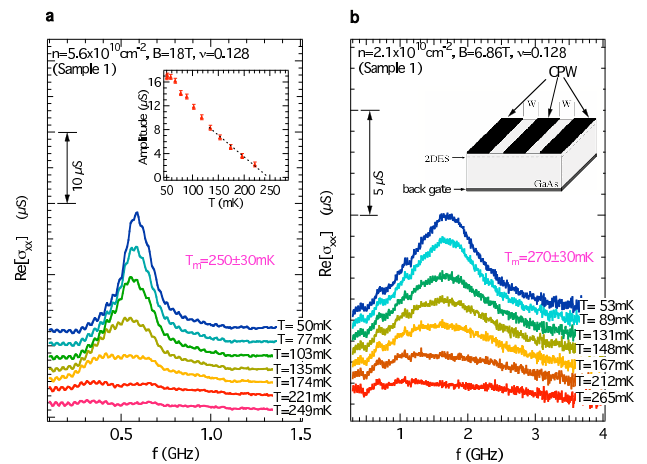


FIG. 1: Temperature (T) dependence of the microwave spectra of the 2D electron solid measured from sample 1 at two different densities (n) with the same Landau filling factor ($\nu = nh/eB$). **a**, T -dependence of the spectra at $n = 5.6 \times 10^{10}$ cm⁻² with $\nu = 0.128$ (magnetic field $B = 18$ Tesla). Spectra at a series of representative T 's are shown and offset for clarity. The pinning resonance of the electron solid observed at $T = 50$ mK is seen to weaken with increasing T and disappear at ~ 250 mK, taken as the melting temperature (T_m) of the electron solid. Inset shows the amplitude of the resonance extrapolates to zero at the similar T_m . **b**, T -dependence of the spectra at $n = 2.1 \times 10^{10}$ cm⁻² with $\nu = 0.128$ ($B = 6.86$ Tesla). The low T resonance disappears at a T_m similar to that shown in **a** ($n = 5.6 \times 10^{10}$ cm⁻²), despite here that n has been reduced by more than a factor of 2 (using a negative voltage between a backgate and the 2DES). Inset shows a schematic of the sample. The dark regions on the top surface represent the coplanar wave guide (CPW). The backgate allows the *in-situ* change of n .

cm⁻², covering a ν range from ~ 0.21 down to ~ 0.03 . Generally, we found T_m to be sensitive to n or B separately (when fixing one and changing the other). On the other hand, near similar ν (changing both n and B while fixing n/B), we have always found T_m to be insensitive to n (or B), within the experimental errors in T_m . Different cooldowns can vary T_m by up to $\sim 15\%$ (at similar ν) but this does not affect our conclusion. We thus find T_m to be mainly determined by ν , so that T_m vs ν as plotted in Fig. 2 defines a melting curve for the electron solid in sample 1. A linear fit of T_m vs ν gives a guide to the eye shown as the dashed line, which lies within 20% from all the (T_m , ν) data points and within 10% from a majority (70%) of them. In the inset of Fig. 2 we plot the “reduced”^{8,18} $t_m = T_m/T_{cm}$ from two similar cooldowns versus ν , where $T_{cm} = e^2\sqrt{n}/(4\pi\epsilon k_B\Gamma)$ is the melting T of a classical 2D electron solid defined earlier (with the value^{7,8} $\Gamma = 127$). In contrast to T_m , t_m can vary significantly (sometimes by a factor of 3) at similar ν . Thus t_m versus ν does not give a well defined melting curve for the electron solid, confirming that T_m is not determined by n or T_{cm} . We have also checked that neither T_m nor t_m plotted against either n

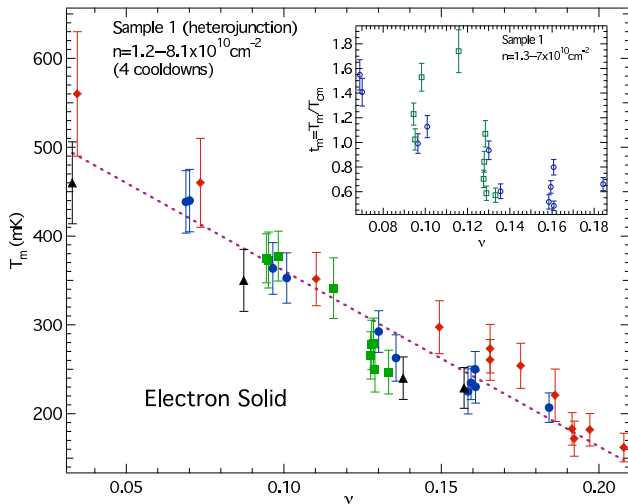


FIG. 2: (T_m, ν) phase diagram for the electron solid in sample 1. The T_m 's are measured in a total of 4 cooldowns (shown as diamonds, circles, squares and triangles), over a wide range of densities ($n=1.2-8.1 \times 10^{10} \text{ cm}^{-2}$) and magnetic fields. Within the experimental uncertainty, T_m versus ν gives rise to a well-defined melting curve of the electron solid. The dashed line is a guide to the eye, obtained by a linear fit through all the data. Typical error bars in T_m are less than 10%. The inset shows the “reduced” t_m versus ν from two cooldowns. t_m is defined as T_m normalized by the classical 2D electron solid melting temperature $T_{cm} = e^2 \sqrt{n} / (4\pi \epsilon k_B \Gamma)$ (where we take $\Gamma=127$). t_m versus ν does not result in a well-defined melting curve, indicating that the melting temperature T_m is not determined by n or T_{cm} .

or B gives any well defined melting curve. We further notice that our measured T_m is also unrelated to the hypothetical “thermal depinning” temperature (T_{depin}) of domains^{15,16,17} of the electron crystal. In fact, one can estimate $T_{\text{depin}} \sim (1/k_B) m_e \omega_0^2 \xi^2 (L/a)^2 \propto n^{3/2}$ (where $\omega_0^2 = 2\pi f_{\text{pk}} eB / m_e \propto n^{-3/2}$ characterizes the “effective pinning potential”¹⁷ (we note that ω_0 is also much larger than $k_B T_m / \hbar$), ξ is the disorder correlation length, $L \propto n$ is the Larkin domain size^{15,16,17} and a is the electron crystal lattice constant), in contrast to T_m , which is determined by ν , and as seen in Fig. 2, typically decreases with increasing n if B is fixed.

Fig. 3 shows the (T_m, ν) melting curve measured on sample 2 (15nm-wide QW). Sample 2 has a tunable $n=2.7-4 \times 10^{10} \text{ cm}^{-2}$. Likely due to the relatively narrow confinement of the 2DES in the QW, sample 2 enters the solid phase for $\nu < 0.3$ and the typical f_{pk} observed is $\sim 6-8$ GHz. In this sample we found T_m again to be controlled by ν , though the value of T_m is higher than in sample 1 at similar ν .

In each of the two samples, at a fixed high- B , T_m typically increases with decreasing n . This is opposite to the classical behavior, where T_{cm} decreases with decreasing n . At a fixed ν , our observed T_m is insensitive to n , and T_m in each sample is a well defined function of ν . Recent theories^{25,26} have suggested that many-body quan-

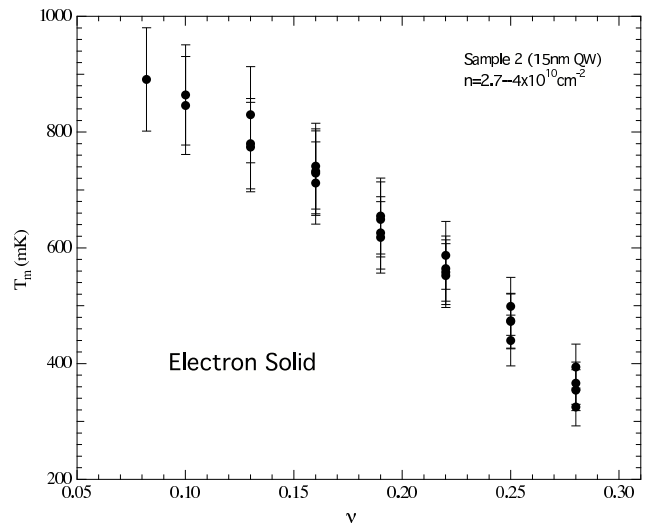


FIG. 3: (T_m, ν) melting curve of the electron solid in sample 2, a narrow QW of width 15 nm. Sample 2 has a tunable $n=2.7-4 \times 10^{10} \text{ cm}^{-2}$ and enters an electron solid phase at $\nu < 0.3$.

tum correlation between electrons can still be important in the solid phase terminating the FQH states at high B . The parameter that captures such quantum correlation is the Landau filling factor $\nu = 2(l_B/r)^2$, which also determines the (single-particle) wavefunction overlap²⁷ between neighboring electrons. This overlap (I_s), given²⁷ by $e^{-(2/\sqrt{3})\pi/\nu}$, is in fact quite small in the high- B , low- ν regime of the MIES. Our data show that T_m is quite strongly dependent on ν (for example, T_m changes by almost a factor of 2 when ν is changed by a factor of 2). Therefore the dependence of T_m on ν is unlikely to result from a T_m that is determined by the Coulomb Hartree energy E_H (which is shown²⁷ to have very weak ν -dependence in this low- ν regime, where the wavefunction overlap I_s has negligible contribution to E_H). Our findings indicate that the melting of MIES is effectively controlled by the inter-electron quantum correlation²⁷, through ν . The well-defined (T_m, ν) melting curve we obtained constitutes the phase boundary between a *quantum solid* and a correlated quantum liquid¹⁵ in each sample.

The T_m we measured in both samples are of similar *order of magnitude* to those in other samples measured previously with various experimental techniques^{18,19,20,21,22,23}. We have noticed that at similar ν , sample 2 (narrow QW) has higher T_m than sample 1 (heterojunction). It has been suggested¹⁶ that the relevant disorder in semiconductor samples that pins the MIES comes mostly from the interfaces vertically confining the 2DES (this is consistent with the relatively high f_{pk} observed in the narrow QW sample). Our findings thus suggest that a 2D electron solid subject to stronger pinning disorder melts at higher T_m , an effect that has been predicted earlier²⁸. We notice, interestingly, that studies on the effects of pinning disorder or geometric

confinement²⁹ on T_m in other solids usually find the opposite behavior. For example, both the vortex solid in a high-temperature superconductor subjected to artificial pinning centers³⁰ and a helium solid in a porous glass³¹ show a depression of T_m with the added disorder. Disorder is generally unavoidable in semiconductor samples, and as seen here can strongly influence the *values* of T_m measured, which may not be those of an ideal, clean Wigner crystal. On the other hand, the observation that in any given sample (thus with fixed intrinsic disorder), T_m is not sensitive to n (nor to B) if $\nu=nh/eB$ is fixed (but is sensitive to n if B is fixed) is difficult to explain in a classical picture of, for example, interplay of disorder and n (screening). The fact that ν being the controlling variable for T_m is found in samples of quite different disorder (including sample 1, in which one can infer from the observed pinning resonance that the Wigner crystal there can possess substantial correlation length^{14,15,16,17}) suggests that such a behavior (T_m being controlled by ν) arises from some mechanism in which many-body quantum correlation between electrons may be important. The exact role of disorder (perhaps involving its interplay with quantum correlation) in determining the value and behavior of T_m remains to be better understood.

It is also interesting to compare the quantum nature of our 2D electron solid to the quantum solids of helium. In a helium solid, the size of atoms is fixed by nature and the quantum parameter is the De Boer parameter¹ $\Lambda \sim h/(a\sqrt{Mv})$ (where M is the atomic mass, a the inter-atomic distance and v the inter-atomic po-

tential strength), which is fixed at fixed n . The T_m of a helium solid is only determined by n . In the case of a 2D electron solid formed in high B , the size of single electron wavefunction (l_B) is readily tunable by B , independently of n . The quantum parameter here is $\nu=nh/eB$ and we have found that T_m of such an electron solid in a given sample (with fixed disorder) is controlled by ν rather than n .

Acknowledgement Financial support of this work was provided by DOE grant no. DE-FG02-05ER46212, the NHMFL in-house research program, and AFOSR. The spectroscopy measurements were performed at the National High Magnetic Field Laboratory, which is supported by NSF Cooperative Agreement No. DMR-0084173 and by the State of Florida. We thank Glover Jones, Tim Murphy and Eric Palm at NHMFL for experimental assistance. We also thank S. T. Chui, R. L. Willett, Kun Yang and C. C. Yu for inspirational discussions, and thank H. A. Fertig and P. B. Littlewood in particular for discussions regarding the thermal depinning temperature of the Wigner crystal.

Competing Interests The authors declare that they have no competing financial interests.

Correspondence Correspondence should be addressed to Y.P.C. (email: yongchen@rice.edu).

* Current address: Richard Smalley Institute for Nanoscale Science and Technology and Dept. of Physics, Rice University, Houston TX 77005, USA

† Current address: Dept. of Physics, University of Maryland, College Park MD 20742, USA

‡ Current address: School of Electrical and Computer Engineering, Purdue University, West Lafayette, IN 47907, USA

¹ Wilks, J. *The Properties of Liquid and Solid Helium* (Oxford, 1967).

² Kim, E. & Chan, M. H. W. Probable observation of a supersolid helium phase. *Nature (London)* **427**, 225-227 (2004).

³ Shayegan, M. Case for the magnetic-field induced two-dimensional Wigner crystal. In Das Sarma, S. & Pinczuk, A. (eds.) *Perspectives in Quantum Hall Effects*, chap. 9 (Wiley and Sons, New York, 1997).

⁴ Grimes, C. C. & Adams, G. Evidence for a liquid-solid phase transition in a classical, two-dimensional sheet of electrons. *Phys. Rev. Lett.* **42**, 795-798 (1979).

⁵ Wigner, E. P. On the interaction of electrons in metals. *Phys. Rev.* **46**, 1002-1011 (1934).

⁶ Thouless, D. Melting of the two-dimensional Wigner lattice. *J. Phys. C* **11**, L189-L190 (1978).

⁷ Morf, R. H. Temperature dependence of the shear modulus and melting of the two-dimensional electron solid.

Phys. Rev. Lett. **43**, 931-935 (1979).

⁸ Chui, S. T. & Esfarjani, K. Finite-temperature two-dimensional Wigner transition. *Phys. Rev. B.* **44**, 11498-11501 (1991).

⁹ Lozovik, Y. E. & Yudson, V. I. Crystallization of a two-dimensional electron gas in a magnetic field. *JETP Lett.* **22**, 11-12 (1975).

¹⁰ Fukuyama, H., Platzman, P. M. & Anderson, P. W. Two dimensional electron gas in a strong magnetic field. *Phys. Rev. B.* **19**, 5211-5217 (1979).

¹¹ Laughlin, R. B. Anomalous quantum Hall effect: An incompressible quantum fluid with fractionally charged excitations. *Phys. Rev. Lett.* **50**, 1395-1398 (1983).

¹² Kivelson, S., Kallin, C., Arovas, D. P. & Schrieffer, J. R. Cooperative ring exchange theory and the fractional quantum Hall effect. *Phys. Rev. B.* **36**, 1620-1646 (1987).

¹³ Tsui, D. C., Stormer, H. L. & Gossard, A. C. Two-dimensional magnetotransport in the extreme quantum limit. *Phys. Rev. Lett.* **48**, 1559-1562 (1982).

¹⁴ Ye, P. D. *et al.* Correlation lengths of the Wigner-crystal order in a two-dimensional electron system at high magnetic fields. *Phys. Rev. Lett.* **89**, 176802 (2002).

¹⁵ Chitra, R., Giamarchi, T. & Le Doussal, P., Dynamical properties of the pinned Wigner crystal, *Phys. Rev. Lett.* **80**, 003827 (1998); Pinned Wigner crystals, *Phys. Rev. B* **65**, 035312 (2002).

- ¹⁶ Fertig, H. A. Electromagnetic response of a pinned Wigner crystal. *Phys. Rev. B.* **59**, 2120-2141 (1999).
- ¹⁷ Fogler, M. M. & Huse, D. A. Dynamical response of a pinned two-dimensional Wigner crystal. *Phys. Rev. B.* **62**, 7553-7570 (2000).
- ¹⁸ Glattli, D. C. *et al.* Experiments on ordering in classical and quantum 2d electron systems. *Surf. Sci.* **229**, 344-351 (1990).
- ¹⁹ Goldman, V. J., Santos, M., Shayegan, M. & Cunningham, J. E. Evidence for two-dimensional quantum Wigner crystal. *Phys. Rev. Lett.* **65**, 2189-2192 (1990).
- ²⁰ Williams, F. I. B. *et al.* Conduction threshold and pinning frequency of magnetically induced Wigner solid. *Phys. Rev. Lett.* **66**, 3285-3288 (1991).
- ²¹ Paalanen, M. A. *et al.* Electrical conductivity and Wigner crystallization. *Phys. Rev. B.* **45**, 13784-13787 (1992).
- ²² Goldys, E. M. *et al.* Magneto-optical probe of two-dimensional electron liquid and solid phases. *Phys. Rev. B.* **46**, 7957-7960 (1992).
- ²³ Kukushkin, I. V. *et al.* Wigner solid vs. incompressible Laughlin liquid: phase diagram derived from time-resolved photoluminescence. *Europhys. Lett.* **23**, 211-216 (1993); Kukushkin, I. V. *et al.* Evidence of the triangular lattice of crystallized electrons from time resolved luminescence, *Phys. Rev. Lett.*, **72**, 3594 (1994).
- ²⁴ Engel, L. W., Shahar, D., Ç. Kurdak & Tsui, D. C. Microwave frequency dependence of integer quantum Hall effect: Evidence for finite-frequency scaling. *Phys. Rev. Lett.* **71**, 2638-2641 (1993).
- ²⁵ Yi, H. & Fertig, H. A. Laughlin-Jastrow-correlated Wigner crystal in a strong magnetic field. *Phys. Rev. B.* **58**, 4019-4027 (1998).
- ²⁶ Chang, C. C., Jeon, G. S. & Jain, J. K. Microscopic verification of topological electron-vortex binding in the lowest Landau-level crystal state. *Phys. Rev. Lett.* **94**, 016809 (2005).
- ²⁷ Maki, K. & Zotos, X. Static and dynamic properties of a two-dimensional Wigner crystal in a strong magnetic field. *Phys. Rev. B.* **28**, 4349-4356 (1983).
- ²⁸ Tsukada, M. Two-dimensional crystallization of the electrons in MOS structures induced by strong magnetic field. *J. Phys. Soc. Jpn.* **42**, 391-398 (1977).
- ²⁹ Christensen, H. O. Confinement effects on freezing and melting. *J. Phys. C* **13**, R95-R133 (2001).
- ³⁰ Paulius, L. M. *et al.* Evolution of the vortex phase diagram in $\text{YBa}_2\text{Cu}_3\text{O}_{7-\delta}$ with random point disorder. *Phys. Rev. B.* **61**, R11910-R11913 (2000).
- ³¹ Beamish, J. R., Hikata, A., Tell, L. & Elbaum, C. Solidification and superfluidity of ^4He in porous vycor glass. *Phys. Rev. Lett.* **50**, 425-428 (1983).